Received 8 September 2023; revised 29 October 2023; accepted 10 November 2023. Date of publication 17 November 2023; date of current version 30 January 2024.

Digital Object Identifier 10.1109/OJAP.2023.3333905

Dual-Band Shared-Aperture Base-Station Antenna Array With Dual Polarization Using Filtering Magnetoelectric Dipole Antenna

ZHI JING XIAO, YUN FEI CAO, JIA SHENG LIN, YU LAN, AND QUAN XUE (Fellow, IEEE)

Guangdong Provincial Key Laboratory of Millimeter-Wave and Terahertz, South China University of Technology, Guangzhou 510641, China

CORRESPONDING AUTHOR: Y. F. CAO (e-mail: yunfeicaoscut@163.com)

This work was supported in part by the National Key Research and Development Program of China under Grant 2021YFA0717500; in part by the Guangdong Basic and Applied Basic Research Foundation under Grant 2023A1515011317; and in part by the Science and Technology Program of Guangzhou under Grant 202201010580.

ABSTRACT This paper presents a dual-band shared-aperture antenna array using a filtering magnetoelectric (ME) dipole antenna for the application of mobile-communication base station. It is realized by interleaving a lower-band (LB) filtering ME dipole antenna operating from 1.7 to 2.8 GHz and four higher-band (HB) patch antennas in the band of 3.3-3.9 GHz. The filtering performance of the proposed ME dipole antenna is realized by U-shaped slots etched on the radiating arms and a cross-shaped microstrip line inside the aperture of the magnetic dipole, and used to realize a high cross-band isolation. The loss caused by the filtering structure is quite low. The gain suppression of the LB filtering ME dipole antenna reaches about 18 dB in the HB. Results demonstrate that both the HB and LB antennas can maintain stable broadside radiation patterns within their operating bandwidths. The magnitude of the cross-band isolation reaches more than 25 dB.

INDEX TERMS Shared-aperture array, filtering antenna, magnetoelectric dipole antenna, dual-band array, base-station antenna.

I. INTRODUCTION

NOWADAYS, many communication systems are in service simultaneously to fulfill the diverse needs of users. Correspondingly, multi-band shared-aperture arrays are necessary to cover 2G/3G/4G/5G bands. However, design of multi-band/dual-band shared-aperture antenna arrays face many problems and challenges. Due to the close distance between different antenna elements, there is very high cross-band interference in the LB antennas and HB antennas, resulting in isolation deterioration and distortion of radiation patterns.

In the past time, researchers have used methods such as designing bowl-shaped antennas, using decoupling frequency-selective surfaces (FSS), using filtering antennas and using low-scattering elements to address these problems. In [1], [2], [3], the LB antennas are designed as bowl-like shapes, and the HB antennas are put inside the bowl-shaped LB antennas. Since the radiators of LB antennas do not block the HB antennas, the radiation patterns of HB antennas are not affected. In [4], [5], [6], LB antenna is put under the HB antennas, and an FSS layer is designed in the middle of the LB antenna and HB antennas. Since the FSS has reflection and transmission characteristics in HB and LB respectively. The interference in HB antenna and LB antenna is reduced substantially, and the array has good radiation patterns. In [7], [8], [9], [10], [11], [12], the out-of-band suppression function of a filtering antenna is used to mitigate the cross-band interference of the dual-band shared-aperture array. In [10], the filtering performance of the LB and HB antennas is achieved by adding filtering stubs to the feeding lines, and the cross-band mutual coupling is mitigated substantially. In [12], several shorted patches are placed in the vicinity of the radiator to realize a LB filtering antenna, and a high cross-band isolation is achieved due to the filtering function of the antennas. A method of reducing the effect of LB radiators on HB antennas by loading RF

chokes on the radiators is proposed in [13] and [14]. In [15] and [16], dual-band antenna arrays are presented by using the radiators of LB antennas as the reflective ground plane of HB antennas. In [17], the HB cavity-backed antenna elements are placed in the middle of each LB loop-shaped radiator. The cavity greatly reduces the impact of the LB radiators on the HB antennas. In [18] and [19], using low-scattering antenna elements to design dual-band arrays. By loading periodic unit cells, the scattering of the LB antenna element in HB is greatly suppressed. The blockage problem of the LB radiating arms to the HB antennas is tackled. Most of the previously published multi-band/dual-band shared-aperture arrays in [1], [2], [3], [4], [5], [6], [7], [8], [9], [10], [11], [12], [13], [14], [15], [16], [17], [18], [19] use dipole, patch or slot antenna elements. Few works use magnetoelectric (ME) dipoles to construct a multi-band aperture-shared array. Actually, ME dipole antennas feature many advantages such as wide bandwidth, high efficiency, high gain and stable radiation pattern [20], [21], [22], [23].

A novel dual-band shared-aperture antenna array with ±45° dual polarization using the filtering ME dipole antenna is proposed. The novelty and contributions of this paper are listed.

1. A novel filtering ME dipole antenna with low structural complexity is presented. A cross-shaped microstrip line is printed in the center of four dipole arms, the original electric field distribution is perturbed, and a new local minima of gain curve is generated. In addition, etching U-shaped slots on four dipole arms to mitigate the out-of-band scattering. Low loss of smaller than 0.2 dB is introduced by the filtering structure of the proposed LB antenna. The proposed LB ME dipole antenna can have less electromagnetic blockage effect on the HB antennas.

2. Using the proposed LB filtering ME dipole antenna and four wideband differentially-fed patch antennas, a dual-band shared-aperture antenna array with dual polarization is presented. For the differentially-fed patch antenna, the coplanar feeding pads of the L-probes are printed on the same plane with the driven patch, which reduces the structural complexity. Wideband performance is realized using the coupling feeding lines and stacked patches. The proposed array can maintain good broadside radiation patterns within the operating bands of 1.7-2.8 and 3.3-3.8 GHz. The magnitude of the cross-band isolation reaches more than 25 dB.

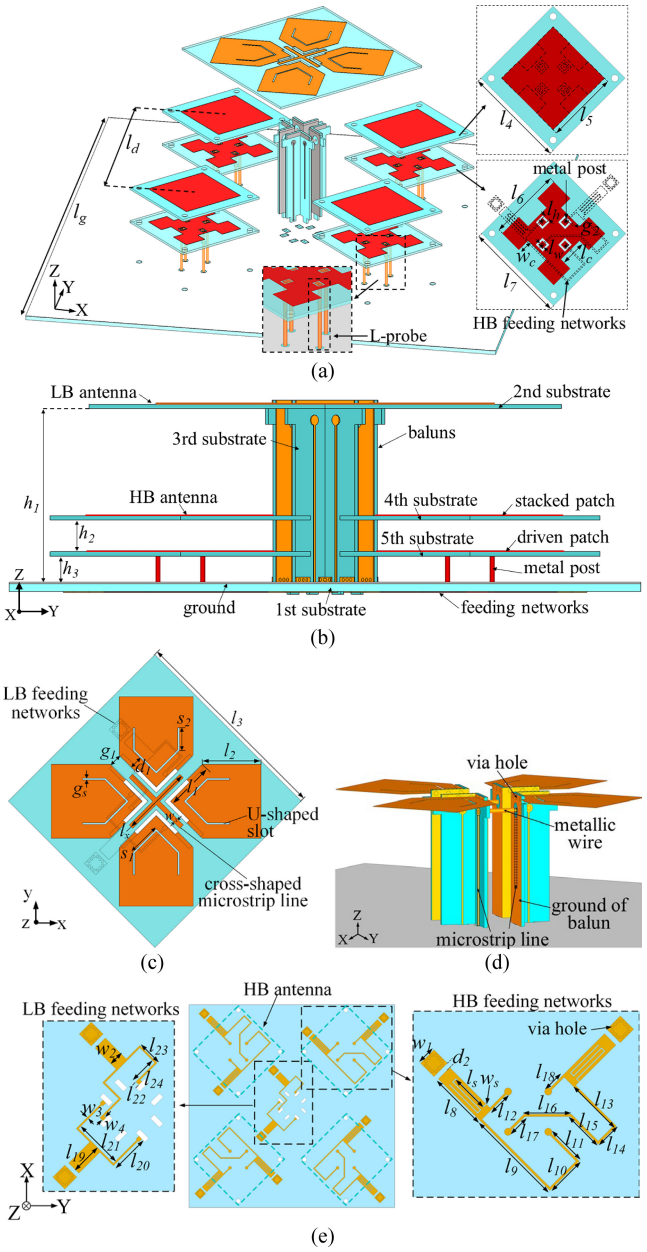

FIGURE 1. Geometry of the proposed antenna array. (a) 3-D view. (b) Side view. (c) LB radiator. (d) Perspective view of the LB baluns. (e) Feeding networks.

II. ANTENNA CONFIGURATION

A. OVERVIEW OF THE DUAL-BAND SHARED-APERTURE ARRAY

Fig. 1(a) shows that the proposed antenna array is composed of an LB ME dipole antenna and four HB patch antennas. All the antennas have ±45° dual polarization. The LB antenna is put in the center of the array, and four HB antennas are put around the LB antenna. Fig. 1(b) shows that the reflective ground plane and feeding networks are designed on the top and bottom layer of the 1st substrate, respectively. Rogers RO4003C is selected as the substrates for fabrication, and the thickness is 0.813 mm.

B. LB ME DIPOLE ANTENNA

Fig. 1(a) shows that the proposed LB antenna has four planar radiating arms, a pair of feeding baluns, a reflective ground and LB feeding networks. All the radiating arms are designed in a pentagonal structure for miniaturization, and they are symmetrically printed on the upper layer of the 2nd substrate. By loading a cross-shaped microstrip line in the center of four planar dipole arms, a local minima of gain curve at 4.1 GHz can be created. Four U-shaped slots are etched on the four planar dipole arms to generate

a local minima of gain curve at 3.4 GHz. Two pairs of perpendicular feeding baluns are below the 2nd substrate. These four radiating arms are connected with the ground plane by the ground of baluns on the vertical 3rd substrates. The gaps between the parallel metal ground of baluns form the magnetic dipoles. The planar dipole arms form the electric dipoles. The ground of balun is printed on one side of the 3rd substrate, and the microstrip feeding line is on the other side, as shown in Fig. 1(d). The horizontal metal wires are used to connect microstrip feeding lines on these two parallel vertical substrates.

The LB feeding networks is shown in Fig. 1(e), which has two power dividers. The ends of the LB power dividers are connected to the vertical microstrip lines of the baluns. By exciting the two power dividers, ±45° dual-polarized radiation can be realized.

C. HB PATCH ANTENNA

The HB dual-polarized patch antenna is made up of a stacked patch, a driven patch, a reflective ground and HB feeding networks, as displayed in Fig. 1(a). The stacked patch is put above the driven patch. Four symmetrical slots are etched on the driven patches. Four coplanar feeding pads are printed inside the corresponding slots, and connected with the feeding networks through vertical metal posts. The feeding pad and the vertical metal post form an L-shaped probe. In this way, the driven patch can be excited by coupling with the feeding pads. Four rectangular opening slots are cut along the edges of the driven patch for miniaturization. In order to achieve high polarization isolation [24], a pair of differential feeding networks is used for feeding the HB antenna, as displayed in Fig. 1(e). 180°-phase-delay line is connected with the HB 1-to-2 power divider.

III. OPERATING PRINCIPLE

A. MECHANISM OF ACHIEVING FILTERING PERFORMANCE OF LB ME DIPOLE ANTENNA

The cross-shaped microstrip line and U-shaped slots can realize the filtering performance of the LB ME dipole antenna.

1) EFFECT OF THE CROSS-SHAPED MICROSTRIP LINE

In order to investigate the function of the cross-shaped microstrip line, two reference antennas (Ant 1 and 2) are compared, as displayed in Fig. 2. Ant 1 is a reference ME dipole antenna. Ant 1 removes the cross-shaped microstrip line and U-shaped slots, and has similar structure with the proposed ME dipole antenna. Ant 2 with a cross-shaped microstrip line is simulated based on Ant 1, and other parts remain unchanged. Fig. 2. plots the realized gain curves of Ant 1, Ant 2 and the proposed LB antenna. A local minima of gain curve is generated at 3.6 GHz in Ant 1. This local minima of gain curve is generated by the feeding baluns, and its working mechanism has been explained in [23]. For Ant 2, a new local minima of gain curve is generated at 4.1 GHz.

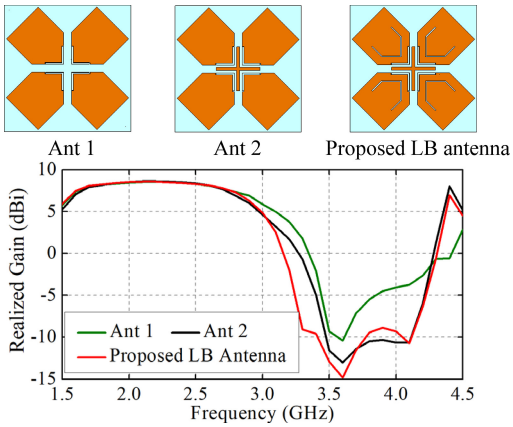

FIGURE 2. Realized gain of Ant 1, Ant 2 and the proposed LB antenna.

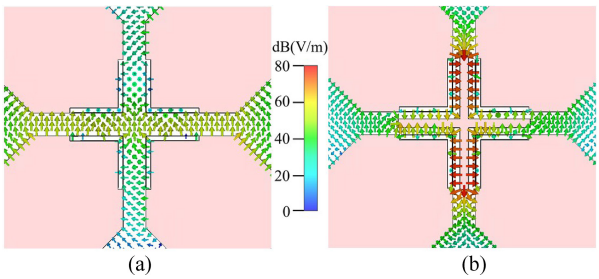

FIGURE 3. Comparison between electric field distribution of (a) Ant 1 and (b) Ant 2 at 4.1 GHz.

To illustrate the operating principle of the cross-shaped microstrip line, the electric field, current distribution and parameter effect are studied. The electric field distributions on the radiators of Ant 1 and Ant 2 at 4.1 GHz are compared, as shown in Fig. 3. When there is no cross-shaped microstrip line, the electric field between the radiation arms is strong, and has half-wavelength distribution. It works as a magnetic dipole for normal radiation. After loading the cross-shaped microstrip line, the original electric field in the magnetic dipole is perturbed. Therefore, there is no RF power radiated at 4.1 GHz, and a local minima of gain curve is created. Fig. 4 shows the current distribution of Ant 2 on the cross-shaped microstrip line at 4.1 GHz. The current accords with half-wavelength distribution on the cross-shaped microstrip line. The cross-shaped microstrip line acts as a bandstop resonator to suppress the radiation at 4.1 GHz. The length (l_x) of the cross-shaped microstrip line is about $\lambda_1/2$, where λ_1 is the guided wavelength at 4.1 GHz. Thus, l_x can be obtained by the following formula:

$$l_x = \lambda_1/2 \tag{1}$$

Fig. 5 displays the effect of $l_x$on the realized gain curve. With l_x increased, the second local minima of gain curve shifts from 4.4 GHz to 4.0 GHz. Therefore, by loading the cross-shaped microstrip line, a local minima of gain curve at 4.1 GHz is produced.

For the LB antenna, l_x is tuned to suppress the radiation at 4.1 GHz, and the frequency bandwidth for the stopband

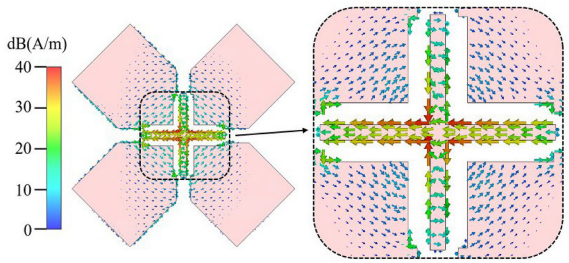

FIGURE 4. The current distribution on the cross-shaped microstrip line of Ant 2 at 4.1 GHz.

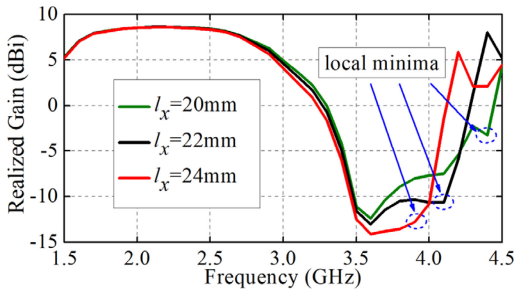

FIGURE 5. Effect of l_x on the realized gain plot of the LB antenna.

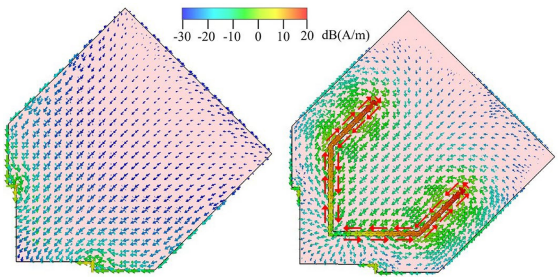

FIGURE 6. The current distribution on the LB radiator at 3.4 GHz. (a) Ant 2 (b) the proposed LB antenna.

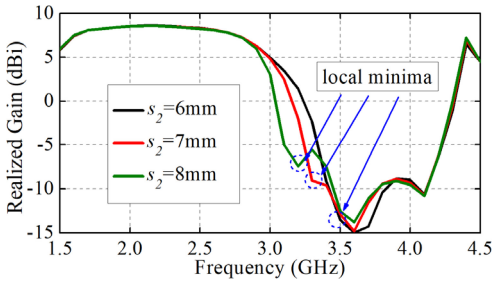

FIGURE 7. Effect of s_2 on the realized gain plot of the LB antenna.

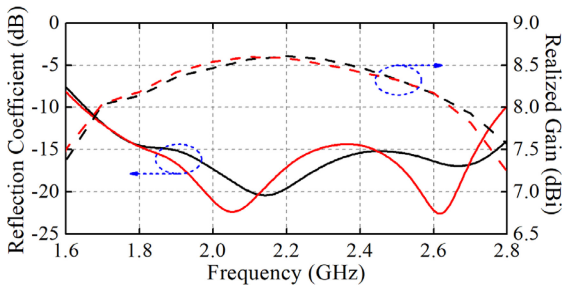

FIGURE 8. Reflection coefficient and realized gain of Ant 1 (black line) and the proposed LB antenna (red line) in the operating band.

suppression is expanded. A high cross-band isolation in the HB of 3.3-3.9 GHz is guaranteed.

2) EFFECT OF THE U-SHAPED SLOT

To introduce another new local minima of gain curve at 3.4 GHz, Ant 2 is modified into the proposed LB antenna. Compared with Ant 2, four U-shaped slots are symmetrical etched on the proposed LB antenna radiator. The proposed LB antenna introduces a new local minima of gain curve at about 3.4 GHz, as displayed in Fig. 2.

To analyze the operating mechanism of the U-shaped slot, the surface current distribution on the dipole arms and parameter effect are investigated. Fig. 6 shows the current distribution at 3.4 GHz on the U-shaped slot of the dipole arm. The current mainly concentrates along the U-shaped slot, and has a half-wavelength distribution. The U-shaped slot on the radiator has bandstop function at 3.4 GHz. The U-shaped slot changes the original current on the electric dipole so that the radiation of the electric dipole is suppressed. The physical length of the U-shaped slot is equal to $2\times(s_1+s_2)$. The U-shaped slot operates in the half-wavelength mode. Its length is about $\lambda_2/2$, where λ_2 is the guided wavelength at 3.4 GHz. Therefore, the length of the U-shaped slot can be obtained by the following formula:

$$2 \times (s_1 + s_2) = \lambda_2/2 \tag{2}$$

Fig. 7 shows the effect of the length of the U-shaped slot on the realized gain. With s_2 decreased from 8 mm to 6 mm, the 1st local minima of gain curve shifts from 3.2 GHz to 3.6 GHz. Therefore, the 1st local minima of gain curve can be controlled by the U-shaped slot.

3) LOSS OF FILTERING STRUCTURE

The loss caused by the filtering structure to the LB antenna is studied. The realized gain curves of Ant 1 and proposed LB antenna are compared, as shown in Fig. 8. For a fair comparison, both antennas are well matched within the band of 1.7-2.8 GHz. The realized gain of the proposed LB antenna with filtering function is very close to that of Ant 1 in the operating frequency band, and the difference of gain is less than 0.2 dB. It means that the filtering structures, i.e., cross-shaped microstrip line and U-shaped slots of the proposed antenna cause small loss. This is a big advantage of the proposed filtering ME dipole antenna.

B. SUPPRESSION OF THE INTERFERENCE BETWEEN LB AND HB ANTENNAS

The stopband radiation suppression property of the proposed LB antenna can reduce its interference to the HB antenna.

The antenna which can reduce the cross-band interference for the dual-band shared-aperture array has high gain suppression performance and low-scattering characteristics in the stopband [18], [19]. Radar cross section (RCS) is

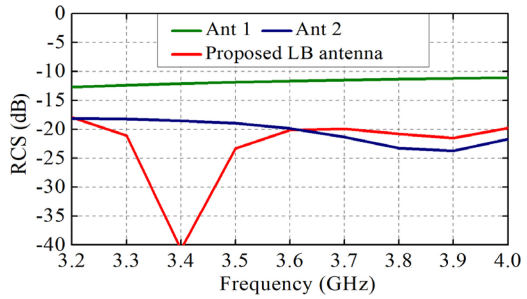

FIGURE 9. RCS curves of Ant 1, Ant 2 and the proposed LB antenna.

an effective index to analyze the scattering characteristic of the antenna. By using the filtering structures, the RCS value of the proposed LB antenna in the band of 3.2-4 GHz can be suppressed substantially. In order to study this, the RCS of Ant 1, Ant 2 and the proposed LB antenna is simulated, as displayed in Fig. 9. The magnitude of RCS of the conventional ME dipole antenna without filtering structures (Ant 1) is about −12 dB. However, after adding filtering structures, the magnitude of RCS is lower than −40 dB in the HB.

Fig. 10 shows the comparison between the proposed array and Array 1. In Array 1, the ME dipole antenna in [23] is used as the LB antenna, which forms a dual-band antenna array together with four HB antennas. Different from Array 1, the proposed filtering ME dipole antenna is used as the LB antenna to complete the proposed array. Fig. 10(b) shows that the radiation patterns of the HB antenna of Array 1 in the xoz plane are deteriorated at 3.5 GHz, and the gain of HB antenna decreases by about 1 dB. The HB antenna in Array 1 has seriously distorted radiation pattern and gain reduction due to the LB antenna. In the proposed array, the radiation patterns of the HB antenna in both xoz and yoz planes are improved. Fig. 10(c) shows the cross-band isolation in these two arrays. The cross-band isolation of the proposed array is higher by about 10 dB than that of Array 1 in the band of 3.3-3.9 GHz. Therefore, using the design in [23] can lead to serious cross-band interference. The proposed LB antenna is more suitable to construct a dual-band shared-aperture antenna array.

Fig. 10(d) shows a comparison of realized gains of Array 1 and the proposed array. For fair comparison, the impedance matching of both arrays is tuned well in the operating bandwidths. The gain in the LB of the proposed array (black line) is very close to that in Array 1 (blue line) from 1.7 to 2.7 GHz. It means that the filtering structures of the proposed LB antenna cause low loss. The gain of the HB antenna in Array 1 (green line) is lower by about 1 dB than that in the proposed array (red line). It is because that the LB antenna without filtering function in Array 1 deteriorates the radiation performance of the HB antennas.

IV. RESULTS AND DISCUSSION

Fig. 11 displays the top view and bottom view of the fabricated antenna array. To validate the proposed method,

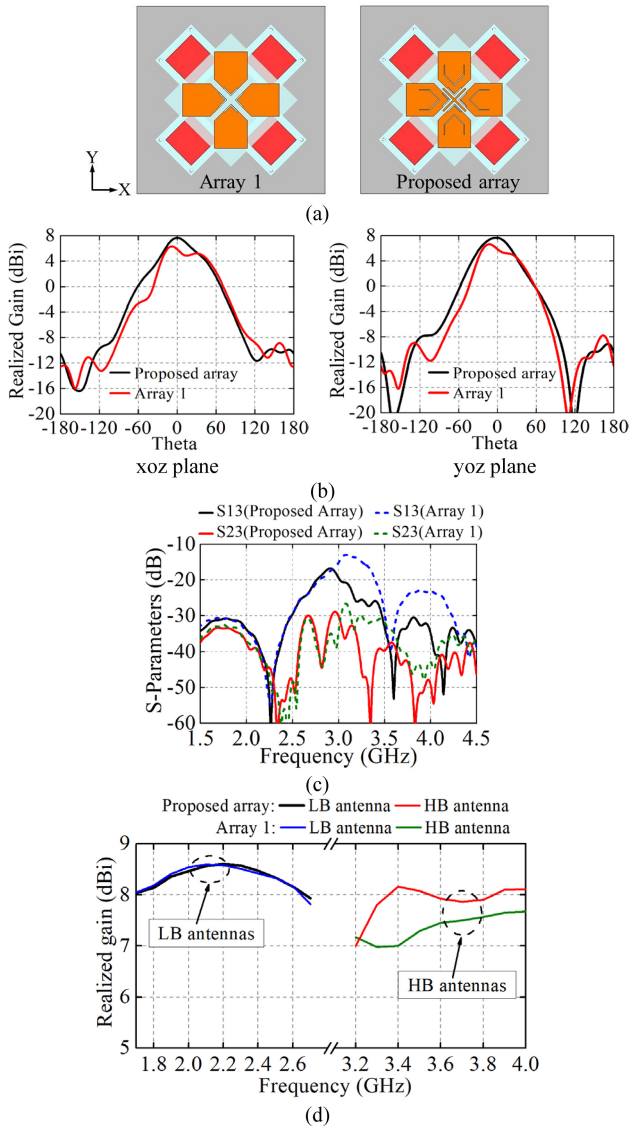

FIGURE 10. (a) Structure of Array 1 and the proposed array. (b) Simulated 2-D radiation patterns of the HB patch antenna in Array 1 and the proposed array at 3.5 GHz. (c) Cross-band isolation of Array 1 and the proposed array. (d) Realized gain curves of Ant 1 and the proposed antenna array.

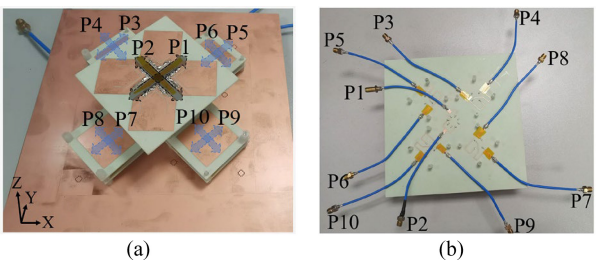

FIGURE 11. Photos of the fabricated proposed dual-band dual-polarized array. (a) Top view. (b) Bottom view.

the antenna array has been measured using the microwave vision group (MVG) StarLab measurement system. Table 1 shows the optimized dimensions of the proposed antenna array. The proposed array has ±45° dual-polarization in both LB and HB.

TABLE 1. Dimensions of the proposed antenna array (Unit: mm).

l_1	l_2	l_3	l_4	l_5	l_6	l_7	l_8	l_9	l_{10}	l_{11}	l_{12}
16	18	63.5	35	25	25	35	12.5	20.8	8.7	8.5	4.5
l_{13}	l_{14}	l_{15}	l_{16}	l_{17}	l_{18}	l_{19}	l_{20}	l_{21}	l_{22}	l_{23}	l_{24}
12.1	5.4	8.3	9.6	4.2	3.7	7	9.3	11.6	5.8	6.3	1.2
l_c	l_d	l_g	l_h	l_s	l_w	l_x	w_1	w_2	w_3	w_4	w_c
9	55	160	2	8.5	2	22	4	3.4	0.4	1	4.5
w_s	w_x	h_1	h_2	h_3	s_1	s_2	d_1	d_2	g_1	g_2	g_s
0.9	1.5	34	6	5	10	7	4	1	4	0.7	0.5

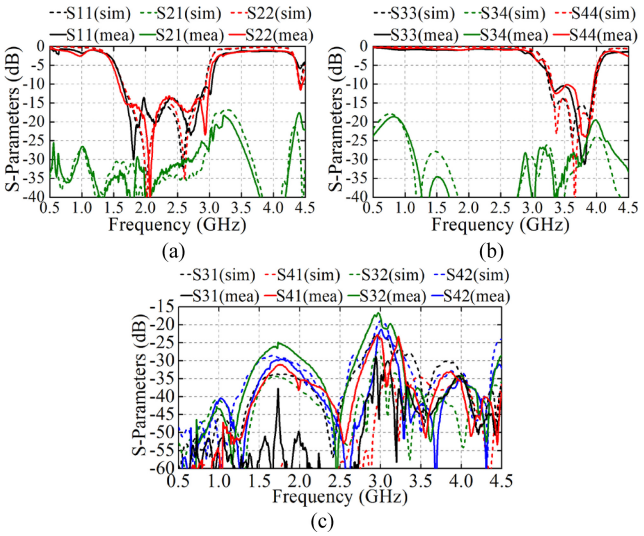

FIGURE 12. Simulated and measured S-parameters of the proposed antenna array. (a) LB antenna. (b) HB antenna. (c) Cross-band isolation.

1) S-PARAMETERS

The S-parameters of the LB antenna in the proposed array are displayed in Fig. 12(a). The simulated and measured operating bandwidths of the LB antenna are 1.64-2.93 GHz (56.5%) and 1.64-2.99 GHz (58.3%) (for S11 < −10 dB), respectively. The measured operating bandwidth of LB antenna is very close to the simulated results. Moreover, there is polarization isolation of over 25 dB between ports P1 and P2 of the LB antenna in the desired operating frequency band. Fig. 12(b) displays the S-parameters of the HB antenna in the proposed array. The simulated and measured bandwidth of HB antenna are 3.3-3.9 GHz (16.7%) and 3.3-3.95 GHz (17.9%), respectively, which are close to each other. There is polarization isolation of higher than 20 dB between ports P3 and P4 of the HB antenna in its operating frequency band. It is worth mentioning that the simulated S-parameters show that the HB antenna has three resonance points within its operating bandwidth, while the measured results exhibit only two resonance points. The difference is caused by the tolerance of fabrication and measurement. Fig. 12(c) demonstrates the port isolation between LB antenna and HB antenna. There is port isolation of higher than 25 dB between LB and HB antennas in both the frequency bands of 1.64-2.93 GHz and 3.3-3.9 GHz. In addition, the reason for the poor cross-band port isolation at 3 GHz is that the out-of-band suppression of the LB antenna is not high enough at 3 GHz.

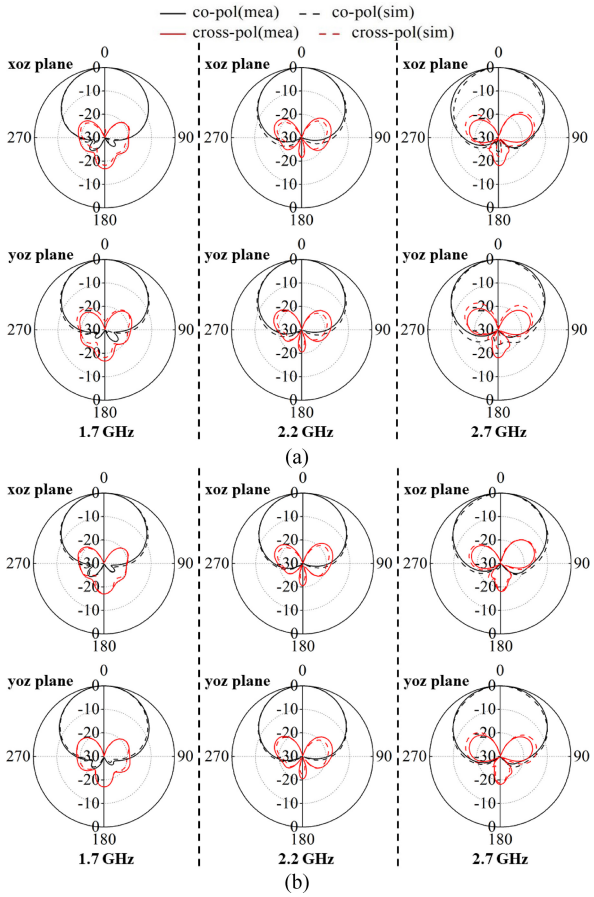

FIGURE 13. Simulated and measured 2-D radiation pattern of the LB antenna of the proposed antenna array. (a) +45°-polarization with port 1 excited. (b) −45°-polarization with port 2 excited.

2) RADIATION PERFORMANCE

Fig. 13(a) and (b) display the ±45° dual-polarization radiation patterns of the LB antenna at 1.7, 2.2 and 2.7 GHz. The 3-dB beamwidth of the LB antenna is 65°±5° in both xoz and yoz planes. The cross-polarization with respect to the co-polarization is lower than −30 dB at the boresight direction. Fig. 14(a) and (b) demonstrate the ±45° dual-polarization radiation patterns of the HB antenna at 3.3, 3.6 and 3.9 GHz. The 3-dB beamwidth of the HB antenna reaches more than 66° in both xoz and yoz planes. At the boresight direction, the cross-polarization with respect to the co-polarization is less than −24 dB. The proposed array has good broadside radiation patterns in both the LB and HB. The simulated and measured radiation patterns agree well.

3) REALIZED GAIN

Fig. 15 plots the realized gains of the proposed array for ±45° dual polarizations. The LB antenna has a flat realized gain of about 8.0 dBi in the operating band of 1.7-2.7 GHz. The out-of-band suppression level reaches about 18 dB in the stopband of 3.3-3.9 GHz. The measured average realized gain of the HB antenna in its operating bandwidth is about 7.4 dBi.

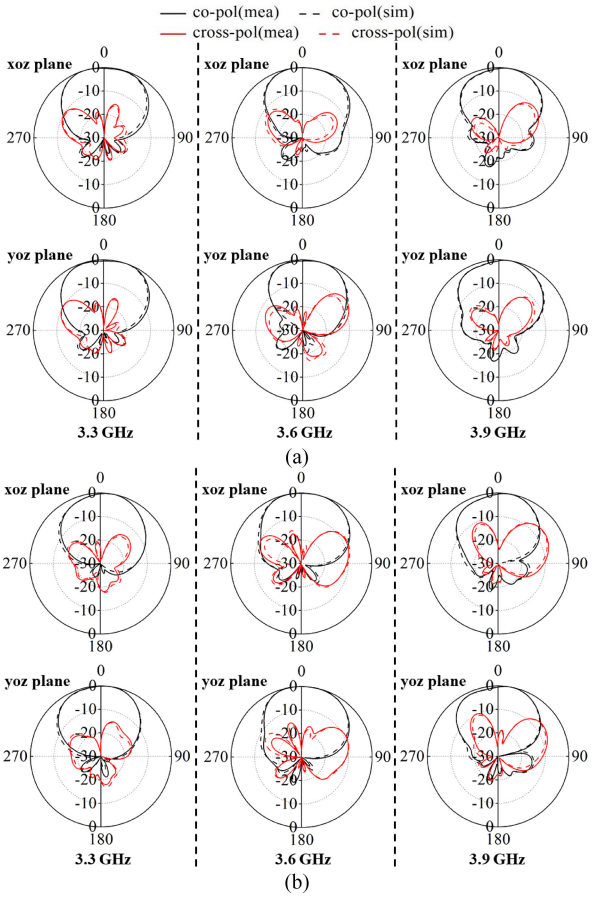

FIGURE 14. Simulated and measured 2-D radiation pattern of the HB antenna of the proposed antenna array. (a) +45°-polarization with port 3 excited. (b) –45°-polarization with port 4 excited.

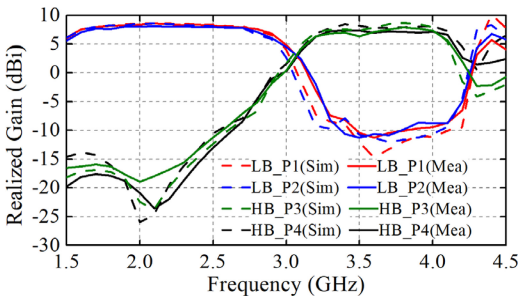

FIGURE 15. Simulated and measured realized gain of the proposed antenna array.

4) COMPARISON WITH OTHER ANTENNA ARRAYS

Table 2 shows the comparison of the proposed array with other dual-band arrays using FSS [4], [5], filtering antennas [7], [8], [9], [10], [11], [12], RF chokes [13], [14]. Compared with the works in [4], [5], [11] and [12], the proposed array has higher cross-band isolation. Compared with the works in [9] and [10], the proposed array has the same cross-band isolation level, but wider operating bandwidths. Besides that, the proposed array has relatively compact size, which is even smaller than that of the works in [5], [10], [12] and [13]. Therefore, the proposed array has good comprehensive performance.

TABLE 2. Comparison with some previous works.

Ref.	Bandwidth/GHz	cross-band iso./dB	Volume/λ_L^3	N_L/N_H
[4]	0.69-0.96; 3.5-4.9	>20	0.7×0.7×0.14	1/4
[5]	0.69-0.96; 3.3-5.0	>18	0.93×0.93×0.17	1/16
[9]	1.65-1.88; 1.89-2.22	> 25	0.65×1.09×0.09	1/1
[10]	2.5-2.7; 3.3-3.6	> 25	0.91×0.91×0.25	1/1
[11]	0.79-0.86; 0.88-0.96	> 18	0.74×0.74×0.23	1/4
[12]	1.71-2.17; 3.3-3.8	> 20	1.1×1.1×0.28	1/4
[13]	1.7-2.26; 3.3-3.7	Not Given	1.02×0.73×0.24	1/4
[14]	0.8-1.0; 1.71-2.28	Not Given	0.76×0.54×0.27	1/4
Pro.	1.62-2.99; 3.3-3.95	> 25	0.86×0.86×0.19	1/4

λ_L: the free-space wavelength at the center frequency of the LB;
iso.: isolation;
N_L/N_H: number of LB/HB elements in the dual-band shared-aperture unit.

V. CONCLUSION

In this paper, a dual-band shared-aperture antenna array with ±45° dual polarization using a filtering ME dipole antenna has been proposed. The proposed filtering structure is integrated on the LB radiating arms, and it greatly reduces the interference of LB antenna to HB antennas. The LB antenna covers 2G/3G/4G frequency bands, and the HB antenna covers 5G frequency band. The proposed array has good broadside radiation patterns, flat gains and high cross-band isolation in the operating bandwidths. Therefore, the proposed antenna array is a good candidate for mobile-communication base-station applications.

REFERENCES

[1] Y. He, Z. Pan, X. Cheng, Y. He, J. Qiao, and M. M. Tentzeris, "A novel dual-band, dual-polarized, miniaturized and low-profile base station antenna," *IEEE Trans. Antennas Propag.*, vol. 63, no. 12, pp. 5399–5408, Dec. 2015.

[2] R. Wu and Q. X. Chu, "A compact, dual-polarized multiband array for 2G/3G/4G base stations," *IEEE Trans. Antennas Propag.*, vol. 67, no. 4, pp. 2298–2304, Apr. 2019.

[3] H. Huang, Y. Liu, and S. Gong, "A novel dual-broadband and dual-polarized antenna for 2G/3G/LTE base stations," *IEEE Trans. Antennas Propag.*, vol. 64, no. 9, pp. 4113–4118, Sep. 2016.

[4] Y. Zhu, Y. Chen, and S. Yang, "Decoupling and low-profile design of dual-band dual-polarized base station antennas using frequency-selective surface," *IEEE Trans. Antennas Propag.*, vol. 67, no. 8, pp. 5272–5281, Aug. 2019.

[5] Y. Zhu, Y. Chen, and S. Yang, "Integration of 5G rectangular MIMO antenna array and GSM antenna for dual-band base station applications," *IEEE Access*, vol. 8, pp. 63175–63187, 2020.

[6] H. Huang, X. Li, and Y. Liu, "A way to improve mutual isolation and radiation pattern of triple-band antenna," *IEEE Antennas Wireless Propag. Lett.*, vol. 21, no. 7, pp. 1433–1436, Jul. 2022.

[7] Y. Li, Z. Zhao, Z. Tang, and Y. Yin, "Differentially fed, dual-band dual-polarized filtering antenna with high selectivity for 5G sub-6 GHz base station applications," *IEEE Trans. Antennas Propag.*, vol. 68, no. 4, pp. 3231–3236, Apr. 2020.

[8] X. Y. Zhang, D. Xue, L. H. Ye, Y. M. Pan, and Y. Zhang, "Compact dual-band dual-polarized interleaved two-beam array with stable radiation pattern based on filtering elements," *IEEE Trans. Antennas Propag.*, vol. 65, no. 9, pp. 4566–4575, Sep. 2017.

[9] M. Li, R. Wang, J. M. Yasir, and L. Jiang, "A miniaturized dual-band dual-polarized band-notched slot antenna array with high isolation for base station applications," *IEEE Trans. Antennas Propag.*, vol. 68, no. 2, pp. 795–804, Feb. 2020.

[10] Y. Liu, S. Wang, N. Li, J. B. Wang, and J. Zhao, "A compact dual-band dual-polarized antenna with filtering structures for sub-6 GHz base station applications," *IEEE Antennas Wireless Propag. Lett.*, vol. 17, no. 10, pp. 1764–1768, Oct. 2018.

[11] W. Duan, Y. F. Cao, Y.-M. Pan, Z. X. Chen, and X. Y. Zhang, "Compact dual-band dual-polarized base-station antenna array with a small frequency ratio using filtering elements," *IEEE Access*, vol. 7, pp. 127800–127808, 2019.

[12] S. J. Yang, R. Ma, and X. Y. Zhang, "Self-decoupled dual-band dual-polarized aperture-shared antenna array," *IEEE Trans. Antennas Propag.*, vol. 70, no. 6, pp. 4890–4895, Jun. 2022.

[13] H. H. Sun, H. Zhu, C. Ding, B. Jones, and Y. J. Guo, "Scattering suppression in a 4G and 5G base station antenna array using spiral chokes," *IEEE Antennas Wireless Propag. Lett.*, vol. 19, no. 10, pp. 1818–1822, Oct. 2020.

[14] H. H. Sun, C. Ding, H. Zhu, B. Jones, and Y. J. Guo, "Suppression of cross-band scattering in multiband antenna arrays," *IEEE Trans. Antennas Propag.*, vol. 67, no. 4, pp. 2379–2389, Apr. 2019.

[15] Y. F. Cao, X. Y. Zhang, and Q. Xue, "Compact shared-aperture dual-band dual-polarized array using filtering slot antenna and dual-function metasurface," *IEEE Trans. Antennas Propag.*, vol. 70, no. 2, pp. 1120–1131, Feb. 2022.

[16] Y. Chen, J. Zhao, and S. Yang, "A novel stacked antenna configuration and its applications in dual-band shared-aperture base station antenna array designs," *IEEE Trans. Antennas Propag.*, vol. 67, no. 12, pp. 7234–7241, Dec. 2019.

[17] Y. Li and Q.-X. Chu, "Coplanar dual-band base station antenna array using concept of cavity-backed antennas," *IEEE Trans. Antennas Propag.*, vol. 69, no. 11, pp. 7343–7354, Nov. 2021.

[18] Y. He, W. Huang, Z. He, L. Zhang, X. Gao, and Z. Zeng, "A novel cross-band decoupled shared-aperture base station antenna array unit for 5G mobile communications," *IEEE Open J. Antennas Propag.*, vol. 3, pp. 583–593, 2022.

[19] W. Niu, B. Sun, G. Zhou, and Z. Lan, "Dual-band aperture shared antenna array with decreased radiation pattern distortion," *IEEE Trans. Antennas Propag.*, vol. 70, no. 7, pp. 6048–6053, Jul. 2022.

[20] L. Siu, H. Wong, and K. Luk, "A dual-polarized magneto-electric dipole with dielectric loading," *IEEE Trans. Antennas Propag.*, vol. 57, no. 3, pp. 616–623, Mar. 2009.

[21] Q. Xue, S. W. Liao, and J. H. Xu, "A differentially-driven dual-polarized magneto-electric dipole antenna," *IEEE Trans. Antennas Propag.*, vol. 61, no. 1, pp. 425–430, Jan. 2013.

[22] K. Luk and B. Wu, "The magnetoelectric dipole—A wideband antenna for base stations in mobile communications," *Proc. IEEE*, vol. 100, no. 7, pp. 2297–2307, Jul. 2012.

[23] S. J. Yang, Y. F. Cao, Y. M. Pan, Y. Wu, H. Hu, and X. Y. Zhang, "Balun-fed dual-polarized broadband filtering antenna without extra filtering structure," *IEEE Antennas Wireless Propag. Lett.*, vol. 19, no. 4, pp. 656–660, Apr. 2020.

[24] H. Wong, K.-L. Lau, and K.-M. Luk, "Design of dual-polarized L-probe patch antenna arrays with high isolation," *IEEE Trans. Antennas Propag.*, vol. 52, no. 1, pp. 45–52, Jan. 2004.